RESEARCH ARTICLE | FEBRUARY 04 2025

Bridging multifluid and drift-diffusion models for bounded plasmas

G. M. Gangemi ; A. Alvarez Laguna ; M. Massot ; K. Hillewaert ; T. Magin

Phys. Plasmas 32, 023502 (2025)
https://doi.org/10.1063/5.0240640

Bridging multifluid and drift-diffusion models for bounded plasmas

Cite as: Phys. Plasmas **32**, 023502 (2025); doi: 10.1063/5.0240640
Submitted: 26 September 2024 · Accepted: 29 December 2024 ·
Published Online: 4 February 2025

G. M. Gangemi,[1,2,a)] A. Alvarez Laguna,[3] M. Massot,[4] K. Hillewaert,[1] and T. Magin[2,5]

AFFILIATIONS

[1]Aerospace & Mechanical Engineering, Université de Liège, Quartier Polytech, Alleé de la Découverte 9, B-4000 Liège, Belgium
[2]Aeronautics and Aerospace, von Karman Institute for Fluid Dynamics, Waterloosesteenweg 72, B-1640 Sint-Genesius-Rode, Belgium
[3]Laboratoire de Physique des Plasmas (LPP), Centre National de la Recherche Scientifique (CNRS), École Polytechnique, Institut polytechnique de Paris, F-91120 Palaiseau, France
[4]Centre de Mathématiques Appliques (CMAP), Centre National de la Recherche Scientifique (CNRS), École Polytechnique, Institut polytechnique de Paris, F-91120 Palaiseau, France
[5]Aero-Thermo-Mechanical Laboratory, Université Libre de Bruxelles, Avenue F.D. Roosevelt 50, B-1050 Brussels, Belgium

[a)]**Author to whom correspondence should be addressed:** giuseppe.gangemi@vki.ac.be

ABSTRACT

Fluid models represent a valid alternative to kinetic approaches in simulating low-temperature discharges: a well-designed strategy must be able to combine the ability to predict a smooth transition from the quasineutral bulk to the sheath, where a space charge is built at a reasonable computational cost. These approaches belong to two families: multifluid models, where momenta of each species are modeled separately, and drift-diffusion models, where the dynamics of particles is dependent only on the gradient of particle concentration and on the electric force. It is shown that an equivalence between the two models exists and that it corresponds to a threshold Knudsen number, in the order of the square root of the electron-to-ion mass ratio; for an argon isothermal discharge, this value is given by a neutral background pressure $P_n \gtrsim 1000$ Pa. This equivalence allows us to derive two analytical formulas for *a priori* estimation of the sheath width: the first one does not need any additional hypothesis but relies only on the natural transition from the quasineutral bulk to the sheath; the second approach improves the prediction by imposing a threshold value for the charge separation. The new analytical expressions provide better estimations of the floating sheath dimension in collisions-dominated regimes when tested against two models from the literature.

I. INTRODUCTION

The accurate simulation of low temperature plasmas (i.e., plasmas with the temperature of heavy species T_h lower than the one of electrons T_e) is crucial to a wide range of aerospace fields, including electronics applications (such as arcing of components used in platforms newly brought to space[1]), hypersonics (like electron transpiration cooling of innovative heat shield for cruise vehicles[2]), electric propulsion,[3] and laboratory plasmas.[4] These applications vary greatly in terms of conditions (thermal non-equilibrium, gas pressure, and so collisionality degree) and in terms of the nature of the species involved (electrons, neutral, and ionized atoms and molecules).

Numerical solutions can be used to infer more information on the physical phenomena and hence improve modeling strategies; the choice of the most appropriate method may depend on the pressure condition of the simulated gas, as shown in Fig. 1. Particle-in-cell (PIC) methods are the most common choice when simulating low-pressure plasmas; these provide a high level of accuracy in the description of the physical phenomena but come with a high computational cost (and a strong direct dependency on the number of particles involved[5–7]). Fluid methods represent an alternative to PIC: while describing the behavior of a gas using macroscopic quantities reduces the accuracy of the representation of the dynamics, their computational cost is significantly lowered. However, coupling the fluid dynamics to the Maxwell equations results in a strongly multi-scaled problem[8] that poses great challenges in the numerical development of a fluid solver, with strict constraints due to the inertia disparity

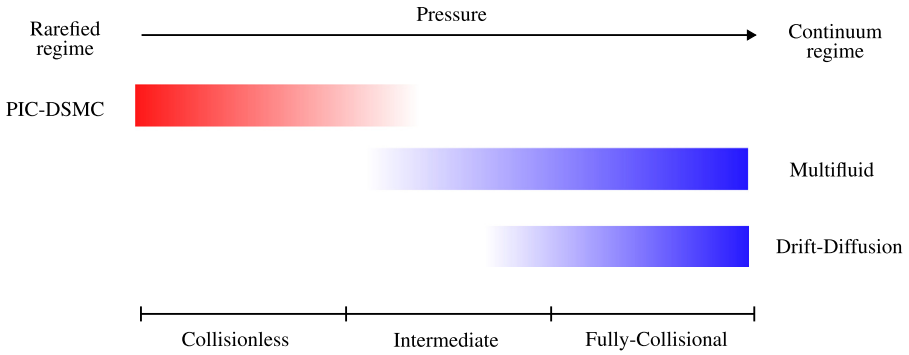

FIG. 1. Qualitative scheme representing the range of applicability of different numerical methods for plasma physics. The gas pressure, increasing from the rarefied to the continuum regime, defines three conditions: collisionless, intermediate, and fully collisional. *Red*: particle method and *blue*: fluid models.

between electrons and heavy species and to the accurate resolution of the Debye length in space-charged regions. Moreover, the description of plasmas with fluid models is directly related to the gas pressure or, in other words, to the collisionality of the plasma.[9] Generally, charged particles in an unmagnetized plasma move under the effect of inertia, thermal motion, electric field, and collisions. In low-pressure regimes, the effect of collisions is negligible so the dynamics of the species is the result of the three remaining terms. A multifluid[8,10] approach is well suited for this condition: each species has its dynamics that is the result of a balance between the inertia, thermal pressure, and electrical forces. Elastic collisions can be introduced with friction terms[11] and become more relevant when the gas pressure is increased. In this regime, drift-diffusion models[12,13] are often used: the electric field (drift) drives most of the motion of the charged particles and diffusion happens due to concentration and temperature gradients. The kinetic derivation of these two models is different. The multifluid approach can be seen as a part of the family of moments method,[14–16] with the governing equations obtained with moments of the Boltzmann equation, truncated with different closure relations. An alternative derivation was proposed by Benilov[17] using the Chapman–Enskog method, but this work was based on the assumption that collision cross sections between particles of different species are significantly smaller than those for collisions between particles of the same species. However, certain interactions, such as charge exchange collisions between ions and neutrals compared to neutral-neutral interactions, violate this assumption, as noted in the paper's conclusions. Drift-diffusion models belong to the family of multicomponent approaches, whose derivation based on the Chapman–Enskog method has been investigated extensively in the past.[18,19] In this case, no assumption on the collision cross sections has to be made, but the full governing equations can be obtained using a scaling obtained from the dimensional analysis of the Boltzmann equation. In addition to the differences in the way the models are derived, authors[9,20] have shown that the momentum equations of the multifluid approach degenerate into the drift-diffusion equations if the dynamics of the particles is assumed dominated by collisions. The minimum gas pressure that results in the "collision-dominated" plasma condition is usually given depending on the plasma considered and the geometrical shape of the domain. To the knowledge of the authors, an indication based on the Knudsen number $\mathrm{Kn} = \lambda/L$, i.e., the ratio of the mean free path λ to a characteristic length of the domain L, is missing.

Fluid models have been used extensively in the simulations of the interaction of the plasma with solid surfaces. When a low-temperature plasma comes in contact with a wall, a region in the proximity of the solid surface, called sheath, develops: the majority of electrons is depleted or repelled and this compensates for the large mobility difference between electrons and positive ions. A potential difference builds up and the wall value adjusts itself, in the case of a floating potential, so no DC flows.[21] The transition from the quasineutral bulk of the plasma to the space charge sheath has been of interest since the first studies on conducting fluids;[22] Bohm[23] derived the criterion that today carries his name, stating that, to have a stable sheath in a mixture of electrons and single-charged ions, the latter must enter the boundary layer region with a speed u_i greater than a limit value $u_B = (k_B T_e/m_i)^{1/2}$, where k_B is the Boltzmann constant and m_i is the ions mass. This condition, valid for a restricted category of plasmas (binary mixture with single-charged ions) and conditions (collisionless), has been the object of several attempts of extension: the interested reader can find an extensive overview of the topic in Baalrud *et al.*[24] To this day, modeling and understanding the effect of elastic collisions on the dynamics of the sheath remains an active challenge for the community. The position where the ions meet the Bohm velocity u_B, or a modified version of it, is conventionally taken as the sheath edge, defining in this way its dimension; through the years, the development of simplified fluid models to describe the dynamics of the charges allowed for obtaining *a priori* estimations of the size of the sheath. Historically, the most used model was the Child–Langmuir law,[9] which evaluates the size of a large voltage sheath; Chabert[21] showed that this formula often underestimates the true size, especially when considering elastic collisions; the author considered isothermal conditions for an argon plasma coupled with the Boltzmann relation for the electrons, with a constant ion mean free path for the collisional term. Benilov[25] provided a summary of the theory of collisionless and collision-dominated sheath. Having an estimation of the dimension of the space-charge region is important for certain applications, such as material processing,[20,21] and for the design of quasineutral solvers to properly characterize the extent of the domain.

As detailed in this introduction, the literature abounds with examples of applications of fluid models to applications where elastic collisions have a relevant role in the dynamics of plasmas, but there is no clear indication on the range of applicability of each approach: this work aims to provide a condition on the Knudsen number of the gas that results in equivalence between the isothermal version of the multifluid and the drift-diffusion models. This value, which is inferred from numerical results, is confirmed by a non-dimensional analysis of the equations. The analysis is performed based on a novel scaling that considers the reduced velocity of charges entering the sheath due to the

increased collisionality. Once the equivalence of the models is established, we use the analytical solutions of the drift-diffusion equations to obtain two analytical formulas to estimate the position of the sheath edge, which correctly predict the size of the sheath at high pressures for both drift-diffusion and multifluid simulations. We can, in this way, investigate the influence of elastic collisions on the position of the sheath edge by using a model, the drift-diffusion one, suited for collisional regimes.

This document is divided as follows: in Sec. II, we describe the fluid models, multifluid and drift-diffusion; the non-dimensional version of the equations is given in Sec. III, followed by the derivation of the analytical solutions of the drift-diffusion equations (Sec. IV). These expressions are used to derive two formulas to estimate the position of the sheath edge (Sec. V). Numerical strategies are described in Sec. VI; the results of the simulations are shown and discussed in Sec. VII. Finally, conclusions are drawn, and future developments are discussed in Sec. VIII.

II. FLUID MODELS

Fluid models describe the behavior of a gas by conservation equations of macroscopic quantities derived as velocity moments of the kth particle velocity distribution function (VDF) $f_k(\mathbf{x}, \mathbf{c}_k, t)$ (with $\mathbf{c}_k$ the kth particle velocity, $\mathbf{x}$ the space coordinate, and t the time). The evolution of this quantity is accounted for using the Boltzmann equation[18] from which governing equations for the velocity moments can be derived through kinetic derivation.

We introduce the governing equations of the two models of interest in this work by first introducing the configuration of the testcase we are going to study, as many hypotheses are strongly connected to the physics we want to simulate. Figure 2 shows the one-dimensional symmetric domain that represents a DC discharge,[9] where a mixture of positive ions i, electrons e, and neutral atoms n is in contact with floating walls (at $x = \pm L/2$, L is the domain length): we consider a weakly ionized plasma; hence, only charges are simulated and the neutrals particles act as a background gas. The plasma is assumed isothermal, with the temperatures constant in time and space but different between heavy species and electrons ($T_h \neq T_e$). Although these hypotheses preclude the simulation of the complete physics of many interesting phenomena, the resulting governing laws are well suited to describe the formation of the sheath: the low-pressure conditions

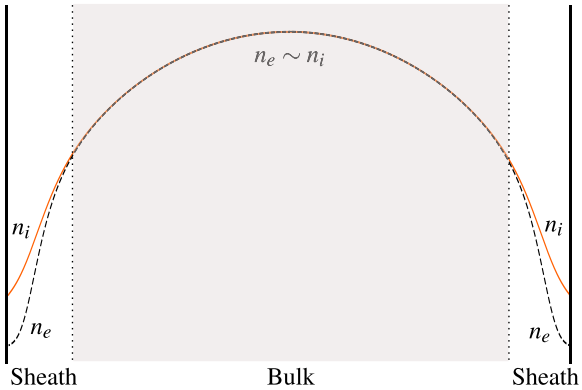

FIG. 2. Schematic of the one-dimensional discharge.

make the energy exchange between the light electrons and heavy particles very inefficient (due to the low number of collisions), and therefore, it is impossible to reach the thermal equilibrium. Multifluid models (lately referred to as "**MF**") represent species inside the plasma as single fluids, each one with its dynamics: interactions between particles are accounted for through source terms. From Alvarez Laguna *et al.*,[11] the dimensional multifluid equations are

$$\partial_t n_e + \partial_x(n_e u_e) = n_e \nu^{iz}, \tag{1a}$$

$$\partial_t n_i + \partial_x(n_i u_i) = n_e \nu^{iz}, \tag{1b}$$

$$\partial_t(n_e u_e) + \partial_x\left[n_e u_e^2 + \frac{p_e}{m_e}\right] = -\frac{n_e q_e}{m_e}\partial_x\phi - n_e(u_e - u_n)\nu_{en}, \tag{1c}$$

$$\partial_t(n_i u_i) + \partial_x\left[n_i u_i^2 + \frac{p_i}{m_i}\right] = -\frac{n_i q_i}{m_i}\partial_x\phi - n_i(u_i - u_n)\nu_{in}, \tag{1d}$$

$$\partial_{xx}^2\phi = -\frac{(q_e n_e + q_i n_i)}{\varepsilon_0}, \tag{1e}$$

where n_k is the kth species number density, u_k the kth species velocity, m_k its mass, and q_k its charge (here $q_e = -q$ and $q_i = q$, with q the elementary charge). The species partial pressure follows the perfect gas law $p_k = n_k k_B T_k$, with T_k the species temperature (T_e for electrons and T_h for ions). Equation (1e) is the Poisson equation with ε_0 the vacuum permittivity. The collision frequencies ν_{en} and ν_{in} account only for elastic collisions between charges and neutrals (in accordance with the hypothesis of a weakly ionized plasma),

$$\nu_{en} = \frac{16}{3} n Q_{en}^{(1,1)} \sqrt{\frac{k_B T_e}{2 m_e \pi}}, \quad \nu_{in} = \frac{8}{3} n Q_{in}^{(1,1)} \sqrt{\frac{k_B T_h}{m_i \pi}} \tag{2}$$

with $Q_{en}^{(1,1)}$ and $Q_{in}^{(1,1)}$ collision integrals[26] obtained from the thermodynamic library Mutation++.[27] Neutrals are assumed at rest; hence, the friction terms in Eqs. (1c) and (1d) simplify to $n_k(u_k - u_n)\nu_{kn} = n_k u_k \nu_{kn}$.

Many authors have used drift-diffusion models (here referred to with "**DD**") for low temperature plasma physics simulations.[13,28–30] The one-dimensional discharge of Fig. 2 can be modeled as a purely diffusive problem; therefore, we have

$$\partial_t n_e + \partial_x(n_e V_e) = n_e \nu^{iz}, \tag{3a}$$

$$\partial_t n_i + \partial_x(n_i V_i) = n_e \nu^{iz}, \tag{3b}$$

$$\partial_{xx}^2\phi = -\frac{(q_e n_e + q_i n_i)}{\varepsilon_0}, \tag{3c}$$

where V_k is the diffusion velocity of the kth species.

Different approaches exist for the modeling of the diffusion velocity; we restrict our analysis to a binary diffusion model,

$$V_k = \left(-\frac{D_k}{n_k}\partial_x n_k - \mu_k \partial_x \phi\right) \tag{4}$$

with species diffusion coefficient D_k and the species mobility μ_k (adapted to include only charge-neutral collisions),

$$D_k = \frac{k_B T_k}{m_k \nu_{kn}}, \quad \mu_k = \frac{q_k}{m_k \nu_{kn}}. \tag{5}$$

This approach includes only binary interactions, losing its accuracy when the mixture grows in complexity, i.e., when the movement of the

single particles is determined by the interaction of multiple species at the same time.

The source term for Eqs. (1a) and (1b) and (3a) and (3b) simulates the effect of electron impact ionization; this value, for isothermal simulations, is an eigenvalue of the problem[31] and requires careful numerical treatment.[10]

Section III introduces the non-dimensional form of the governing equations, with a novel value for the reference velocity that includes the slowing down effects of the elastic collisions.

III. SCALED EQUATIONS

The Bohm velocity u_B is often taken as the reference value for the velocity of the charges entering the sheath,[10,24,32] although, in case the collisionality increases, it overestimates the actual speed that is reduced to the slowing effect caused by the interactions with the background gas.[9]

Therefore, we start by proposing a new reference velocity,

$$u_0 = \alpha u_B = \alpha\sqrt{\frac{k_B T_e}{m_i}}, \tag{6}$$

and introduce additional reference quantities,

$$\bar{n} = n/n_0, \quad \bar{x} = x/L_0, \quad \bar{\phi} = \phi/\phi_0, \tag{7}$$

where $n_0 = n_{e0}$ is the reference number density (and n_{e0} the initial electron number density), L_0 is a reference length, and the reference potential is defined as $\phi_0 = k_B T_e/q$ (i.e., the electron temperature in eV). The parameter α, whose value will be defined in Sec. VII B, acts as a scaling parameter on u_0: in the collisionless limit, the reference value should tend to the collisionless Bohm velocity $u_0 = u_B$, hence $\alpha = 1$; as the charges collision frequencies increase, α should decrease, reflecting the reduced speed of particles. The scaled elastic collision frequencies of electrons and ions, from Eq. (2), depend on the kth charges-neutral Knudsen number $\mathrm{Kn}_{kn} = \lambda_{kn}/L_0$ [with $\lambda_{kn} = (n_n Q_{kn}^{(1,1)})^{-1}$ the mean free path that a charged particle travels between each interaction with the neutral background gas],

$$\nu_{en} = \bar{\nu}_{en} t_0^{-1} = \frac{16}{3\sqrt{2\pi}} \underbrace{n_n Q_{en}^{(1,1)} L_0}_{\mathrm{Kn}_{en}^{-1}} \frac{\alpha^{-1}}{\sqrt{\varepsilon}} \underbrace{\left[\frac{u_0}{L_0}\right]}_{t_0^{-1}} = \frac{16}{3\sqrt{2\pi}} \frac{t_0^{-1}}{\alpha\sqrt{\varepsilon}\mathrm{Kn}_{en}}, \tag{8a}$$

$$\nu_{in} = \bar{\nu}_{in} t_0^{-1} = \frac{8\sqrt{\kappa}}{3\sqrt{\pi}} \underbrace{n_n Q_{in}^{(1,1)} L_0}_{\mathrm{Kn}_{in}^{-1}} \alpha^{-1} \underbrace{\left[\frac{u_0}{L_0}\right]}_{t_0^{-1}} = \frac{8\sqrt{\kappa}}{3\sqrt{\pi}} \frac{t_0^{-1}}{\alpha \mathrm{Kn}_{in}}, \tag{8b}$$

where we introduced the electron-to-ion mass ratio $\varepsilon = m_e/m_i$, the temperature ratio $\kappa = T_h/T_e$, and a reference timescale t_0. We can now write the scaled version of Eq. (1),

$$\partial_t \bar{n}_e + \partial_{\bar{x}}[\bar{n}_e \bar{u}_e] = \bar{n}_e \bar{\nu}^{iz}, \tag{9a}$$

$$\partial_t \bar{n}_i + \partial_{\bar{x}}[\bar{n}_i \bar{u}_i] = \bar{n}_e \bar{\nu}^{iz}, \tag{9b}$$

$$\partial_{\bar{x}}\left[\bar{n}_e\left(\bar{u}_e^2 + \frac{1}{\varepsilon\alpha^2}\right)\right] = \frac{\bar{n}_e}{\varepsilon\alpha^2}\partial_{\bar{x}}\bar{\phi} - \frac{16}{3\sqrt{2\pi}}\frac{\bar{n}_e \bar{u}_e}{\alpha\sqrt{\varepsilon}\mathrm{Kn}_{en}}, \tag{9c}$$

$$\partial_{\bar{x}}\left[\bar{n}_i\left(\bar{u}_i^2 + \frac{\kappa}{\alpha^2}\right)\right] = -\frac{\bar{n}_i}{\alpha^2}\partial_{\bar{x}}\bar{\phi} - \frac{8}{3\sqrt{\pi}}\frac{\bar{n}_i \bar{u}_i\sqrt{\kappa}}{\alpha \mathrm{Kn}_{in}}, \tag{9d}$$

$$\partial^2_{\bar{x}\bar{x}}\bar{\phi} = \chi^{-1}(\bar{n}_e - \bar{n}_i), \tag{9e}$$

and Eq. (3),

$$\partial_t \bar{n}_e + \frac{3\sqrt{2\pi}}{16}\frac{\mathrm{Kn}_{en}}{\alpha\sqrt{\varepsilon}}\partial_{\bar{x}}\left[-\partial_{\bar{x}}\bar{n}_e + \bar{n}_e\partial_{\bar{x}}\bar{\phi}\right] = \bar{n}_e\bar{\nu}^{iz}, \tag{10a}$$

$$\partial_t \bar{n}_i + \frac{3\sqrt{\pi}}{8}\frac{\alpha\mathrm{Kn}_{in}}{\sqrt{\kappa}}\partial_{\bar{x}}\left[-\kappa\partial_{\bar{x}}\bar{n}_i - \bar{n}_i\partial_{\bar{x}}\bar{\phi}\right] = \bar{n}_e\bar{\nu}^{iz}, \tag{10b}$$

$$\partial^2_{\bar{x}\bar{x}}\bar{\phi} = \chi^{-1}(\bar{n}_e - \bar{n}_i), \tag{10c}$$

where $\chi = (\lambda_D/L_0)^2 = (\varepsilon_0 k_B T_e)/(n_{e0} q_e^2 L_0^2)$ is the non-dimensional (initial) Debye length squared. The notation $\bar{(\cdot)}$ for non-dimensional quantities will be abandoned in the rest of the paper for the sake of clarity: when not otherwise specified, all quantities will be considered non-dimensional.

We can now obtain analytical expressions for the drift-diffusion equations.

IV. ANALYTICAL PROFILES

Starting from the steady state form of Eq. (3),

$$\frac{1}{\varepsilon\bar{\nu}_{en}}\partial_x(-\partial_x n_e + n_e\partial_x\phi) = n_e\nu^{iz}, \tag{11a}$$

$$\frac{1}{\bar{\nu}_{in}}\partial_x(-\kappa\partial_x n_i - n_i\partial_x\phi) = n_e\nu^{iz}, \tag{11b}$$

$$\partial^2_{xx}\phi = \chi^{-1}(n_e - n_i), \tag{11c}$$

where we kept the adimensional collision frequency as $\bar{\nu}_{kn}$ for the clarity of the next passages. The bulk solution can be obtained by assuming quasineutrality ($\chi = \lambda_D/L \to 0$), so the Poisson equation [Eq. (11c)] reduces to $n_e = n_i = n$. Subtracting Eq. (11b) from Eq. (11a) and using the quasineutrality assumption, we obtain

$$\partial_x(-\partial_x n + n\partial_x\phi) - \frac{\bar{\nu}_{en}\varepsilon}{\bar{\nu}_{in}}\partial_x(-\kappa\partial_x n - n\partial_x\phi) = 0.$$

This can be rearranged into

$$\partial_x(\partial_x n) = \gamma\partial_x(n\partial_x\phi), \quad \gamma = \frac{\bar{\nu}_{in} + \varepsilon\bar{\nu}_{en}}{\bar{\nu}_{in} - \varepsilon\kappa\bar{\nu}_{en}}, \tag{12}$$

which can be easily integrated twice, with the proper boundary conditions ($\partial_x\phi(x=0) = 0, \phi(x=0) = 0$), to obtain

$$n(\phi(x)) = n_C \exp(\gamma\phi), \tag{13}$$

which is a modified version of the electron Boltzmann relation,[9] with n_C being the value of plasma density at the center of the domain [$n(\phi(x=0)) = n_C$]. One can easily verify that $\gamma - 1 \sim 10^{-3}$ for our simulation conditions (we will nevertheless keep it in the following derivations to avoid singularities).

We can now substitute Eq. (13) in Eq. (11a) and rearrange

$$\frac{1}{\varepsilon\bar{\nu}_{en}}\partial_x[-\partial_x(n_C\exp(\gamma\phi)) + n_C\exp(\gamma\phi)\partial_x\phi] = n_C\exp(\gamma\phi)\nu^{iz},$$

which simplifies to

$$\begin{aligned} \partial^2_{xx}\phi + \gamma(\partial_x\phi)^2 &= \frac{\varepsilon\bar{\nu}_{en}\nu^{iz}}{1-\gamma}, \\ \partial_x\phi|_{x=0} &= 0, \\ \phi|_{x=0} &= 0, \end{aligned} \tag{14}$$

where we highlighted the boundary conditions. If we consider the ionization frequency ν^{iz} constant (a reasonable assumption as all the quantities have reached steady state), Eq. (14) has an analytical solution,

$$\phi(x) = \frac{\ln[\cos(\xi x)]}{\gamma}, \quad \xi = \sqrt{\frac{(\nu_{in} + \varepsilon\nu_{en})\nu^{iz}}{\kappa + 1}}. \tag{15}$$

One can see that Eq. (13) then becomes

$$n(x) = n_C \cos(\xi x). \tag{16}$$

Equation (16) reminds the model developed by Schottky;[33] however, in our work, we do not impose plasma vanishing density at the wall (the often called "Schottky condition") and the results comes directly from the governing equations and the quasineutrality assumption.

Figure 3 shows the electric potential obtained at different levels of collisionality using Eq. (15). The analytical profiles reach an asymptote, and they do not extend to the wall (positioned at $x = L/2 = 50\lambda_D$). In the proximity of the sheath edge, where the quasineutrality is lost, the solution loses its basis. This aspect, often seen as a limitation, is used in Sec. V to find the position of the sheath edge, as the classical Bohm criterion is not valid in collision-dominated regimes.

V. ESTIMATION OF THE SHEATH WIDTH

Two different methods are proposed here to define a unique sheath edge for collisional plasma as follows:

1. Finding the position of the vertical asymptote of Eq. (15). This approach is free of assumptions but provides less accurate results.

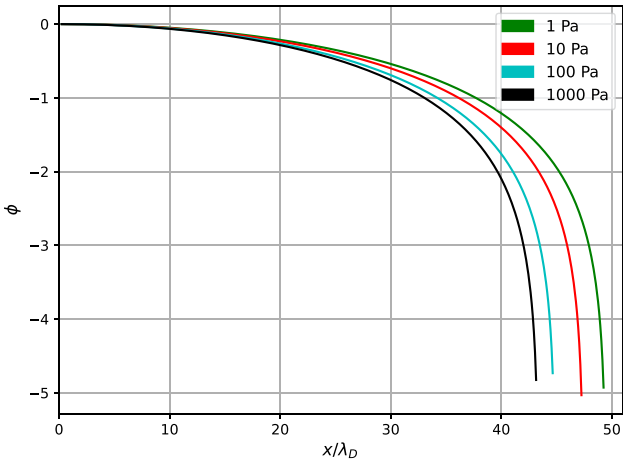

FIG. 3. Analytical profile of the electric potential obtained with Eq. (14) at different background pressures (*green*: 1 Pa, *red*: 10 Pa, *cyan*: 100 Pa, and *black*: 1000 Pa).

2. Computing $\partial^2_{xx}\phi$, we can impose a charge density limit value $\bar{\rho}_C$ (following the intuition of Beving *et al.*[32]) for when the plasma loses its neutrality. This method allows for more accurate results but is dependent on the arbitrary choice of the threshold value $\bar{\rho}_C$.

The computation of the vertical asymptote of Eq. (15) is straightforward,

$$x^{As} = \lim_{\phi\to-\infty} \frac{\cos^{-1}(\exp[\gamma\phi])}{\xi} = \frac{\pi}{2\xi}. \tag{17}$$

This value depends only on fluid quantities and is based only on the quasineutral assumption. The procedure followed here is similar to the one used by Riemann and co-workers[31,34] but rises naturally from a different set of equations.

A second formula can be obtained by quantifying the deviation from the quasineutrality by introducing a measure of the charge density $n_e\bar{\rho}_C = (n_i - n_e)$: a threshold value $\bar{\rho}_C$ is obtained from collisionless ($\nu_{en} = \nu_{in} = 0$) multifluid solution on our setup, taking the charge density at the position where $u_i = u_B$. Inserting Eq. (15) in the scaled Poisson equation Eq. (11c), we have

$$-\chi\partial^2_{xx}\phi = n_e\bar{\rho}_C = n_i - n_e = \frac{\xi^2\chi}{\cos^2(\xi x)}, \tag{18}$$

which can be easily rearranged to obtain

$$x^{\rho} = \frac{1}{\xi}\cos^{-1}\left(\xi\sqrt{\frac{\chi}{n_e\bar{\rho}_C}}\right). \tag{19}$$

We will test the quality of the predictions from Eqs. (17) and (19) with our numerical solutions in Sec. VII.

VI. NUMERICAL METHODS

We do not describe the details of the space discretization for all the schemes proposed when their use is widely known and not different from the applications in classical fluid dynamics; on the other hand, this section focuses on the time integration schemes used, as their choice is fundamental in the development of the solvers. All simulations have been performed on the same one-dimensional domain, divided into 602 cells: the grid is finer in the proximity of the wall ($\Delta x_{\min} = 0.1\lambda_D$) and becomes gradually coarser in the center of the domain ($\Delta x_{\max} = 0.5\lambda_D$).

A. Multifluid

The implementation of the multifluid equations has been extensively described and validated.[10,11] For the results in this work, we use Roe numerical flux[35] with third-order reconstruction of the solution;[36] the electric potential is obtained by solving the Poisson equation at any time step using centered finite differences. The electron plasma frequency imposes strict constraints for explicit schemes but this does not impact heavily the computational cost of the simulation, provided that the stability constraint imposed by the Courant–Friedrichs–Lewy (CFL) number is respected (CFL < 1). For our simulations, we set CFL = 0.9.

B. Drift-diffusion

A first-order backward Euler has been implemented to solve for Eqs. (3a)–(3c). We focus here on the electron diffusion flux (but the

same reasoning can be applied to the other species), rewriting it in non-conservative form, with indices $\{n+1,\ n,\ n-1\}$ indicating the time step at which the considered quantity is evaluated,

$$\partial_x\left(-\partial_x n_e^{n+1} + n_e^{n+1}\partial_x\tilde{\phi}\right) = -\left(\partial_{xx}^2 n_e\right)^{n+1} + \left(\partial_x n_e\right)^{n+1}\left(\partial_x\tilde{\phi}\right) + \left(n_e\right)^{n+1}\left(\partial_{xx}^2\tilde{\phi}\right). \quad (20)$$

In this way, the expression is linear with the number density and so the system of equations,

$$\left(\frac{\mathbf{I}}{\Delta t} + \mathbf{A}^n\right)\mathbf{U}^{n+1} = \frac{\mathbf{I}}{\Delta t}\mathbf{U}^n + \mathbf{S}^n, \quad (21)$$

is tridiagonal [$\mathbf{A}^n$ is the matrix resulting from discretizing Eq. (20) using centered finite differences] and can be solved using the fast Thomas algorithm. $\mathbf{U}^k = \{n_e, n_i\}^{\mathrm{T}}$ is the variable vector evaluated at time t^k; similarly, the source vector is $\mathbf{S}^k = \left\{n_e^k\nu^{iz}, n_e^k\nu^{iz}\right\}^{\mathrm{T}}$, with ν^{iz} assumed constant during the time step. In Eq. (20), the derivatives of the potential ϕ are not evaluated at $t^{n+1} = t^n + \Delta t$ (with Δt the time step), which will require solving the Poisson equation coupled to the system, but instead a *prediction* of the value $\tilde{\phi}$ is used; this allows to obtain greater stability without increasing excessively the computational cost. This value is obtained by solving

$$-\partial_x\left[\left(\chi - \Delta t\sum_{j\in S}|q_j|\frac{n_j^n}{\nu_{jn}}\right)\partial_x\tilde{\phi}\right] = \sum_{j\in S} q_j\left(2n_j^n - n_j^{n-1}\right) + \Delta t\partial_x\left(|q_j|\frac{n_j^n}{\nu_{jn}}\partial_x\phi^n\right), \quad (22)$$

where S is the species set. The steps to obtain the previous equation are detailed in Hagelaar[37] and have been adapted to our governing laws; the discretized system is tridiagonal and solved using the Thomas algorithm. Figure 4 shows the quality of this method: the procedure gives an accurate prediction, improving the stability of the scheme. All the simulations have been obtained with the same time step used in the multifluid approach.

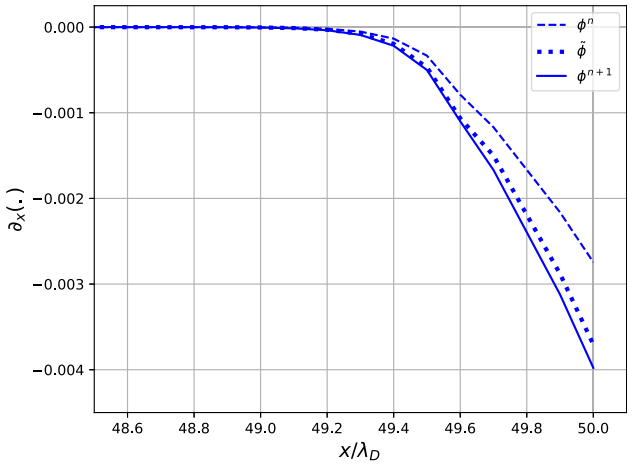

FIG. 4. Gradient of the electric potential ϕ evaluated at time step n (dashed), $n+1$ (full) and the predicted value obtained with Eq. (22) (dots). Values obtained at the first steps of the simulation.

C. Boundary conditions

The correct imposition of the boundary conditions is fundamental for an accurate description of the sheath formation. It is standard,[10,11] for the multifluid modeling, to impose the electron flux to be equal to the number of particles crossing the plane with velocity directed to the wall,

$$n_e u_e\left(x = \pm\frac{L}{2}, t\right) = \pm\frac{1}{4}n_e\sqrt{\frac{k_B T_e}{m_e}} = \pm\frac{n_e}{\sqrt{2\pi\varepsilon}}u_B. \quad (23)$$

The prescribed value is imposed using the ghost cells method[11] and is obtained assuming a Maxwellian VDF. The electron VDF is usually far from equilibrium in the proximity of the wall, due to the reduced number of collisions and to the particles lost at the absorbing surface, and this deviation should be considered in the development of future boundary conditions for fluid models to capture these kinetic effects. Electron and ion density and the ion flux have a Neumann boundary condition.

Setting the boundary conditions to the drift-diffusion model presents substantial differences compared to the multifluid counterpart. Due to the absence of an equation for the electron momentum, we are going to impose a fixed out-going flux to the diffusion velocity,

$$\frac{1}{\varepsilon\bar{\nu}_{en}}\left(-\frac{\partial_x n_e}{n_e} + \partial_x\phi\right) = \frac{1}{\sqrt{2\pi\varepsilon}}, \quad (24)$$

where we scaled with u_B both sides. Approximating the number density gradient with a first-order finite difference formula and the interface number density with the mean of the ghost cell value n_e^G and the last (inside) cell n_e^L,

$$\partial_x n_e = \frac{n_e^G - n_e^L}{\Delta x}, \quad n_e = \frac{n_e^G + n_e^L}{2}, \quad (25)$$

and, rearranging, we obtain

$$n_e^G = n_e^L\frac{1 + \frac{\Delta x}{2}\left(\partial_x\phi - \bar{\nu}_{en}\sqrt{\frac{\varepsilon}{2\pi}}\right)}{1 - \frac{\Delta x}{2}\left(\partial_x\phi - \bar{\nu}_{en}\sqrt{\frac{\varepsilon}{2\pi}}\right)}. \quad (26)$$

Equations (23) and (26) can be extended easily using the scaling in Sec. III; we will see in Sec. VII that our choice does not impact the results of the simulations. Ion density has a Neumann boundary condition.

Finally, we impose a floating boundary condition for the electric potential.

D. Ionization frequency

We use an iterative formula[10] to obtain a steady-state value of the ionization frequency,

$$\nu^{iz} = \frac{|n_i u_i|_{x=-L/2} + |n_i u_i|_{x=L/2}}{\int_L n_e dx} \quad (27)$$

TABLE I. Argon discharge conditions.

Initial electron number density	n_{e0}	1×10^{16} m^{-3}	Ion (Heavy-species) temperature	T_h	0.05 eV
Electron temperature	T_e	2 eV	Ion-neutral collision integral	$Q_{in}^{(1,1)}$	1.41×10^{-18} m^2
Electron-neutral collision integral	$Q_{en}^{(1,1)}$	7×10^{20} m^2	Electron-to-ion mass ratio	$\varepsilon = m_e/m_i$	1.36×10^{-5}
Ion-to-electron temperature ratio	$\kappa = T_h/T_e$	0.025	Initial Debye length	λ_D	10^{-4} m
Squared non-dimensional initial Debye length	$\chi = \lambda_D^2/L_0^2$	1	Discharge width	L	10^{-2} m

with, for **DD**, the ion diffusive flux $|n_i V_i|_{x=\pm L/2}$ to account for the outgoing flux. In this way, the number of particles reinjected in the domain is proportional to the flux of ions to the wall and maintains the electron population constant in the domain.

VII. RESULTS

Table I shows the important quantities and non-dimensional parameters used for the simulations. Various collisional regimes were investigated; the number density n of the gas is chosen as $n \sim n_n = p_n/(k_B T_h)$ so, varying the background pressure, we can vary the number of elastic collisions. Figure 5 and Table II detail the conditions of four regimes: we are showing two of these, ranging from an almost collisionless plasma to a dynamics fully dominated by elastic collisions.

A. Numerical comparison

We compare solutions from the multifluid and drift-diffusion approach in terms of number density, (diffusion) velocity, and electric potential profiles. The number density is scaled with the value at the center of the bulk $[n_k(x=0)]$; velocity values are presented in non-dimensional form using the classic (collisionless) Bohm velocity; and finally, the electric potential is shown scaled with ϕ_0. All quantities are obtained at steady state condition, chosen as the moment when $||\mathbf{U}^{n+1} - \mathbf{U}^n|| < 10^{-4}$.

Figure 6 presents the profiles of the electrons and ions number densities: all the models can provide continuous solutions from the bulk region (where the chosen scaling allows to overcome the differences in the modeling of the ionization frequency) to the space charge region close to the boundary. As expected, the profiles differ significantly in the more rarefied regime: in this condition, the convective term of Eq. (9) is still relevant and the **DD** model cannot capture correctly the dynamics of the particles. As the number of collisions increases, the movement of the charges becomes dominated by the interaction with the background gas, with the prediction from the diffusion model getting closer to the multifluid profile.

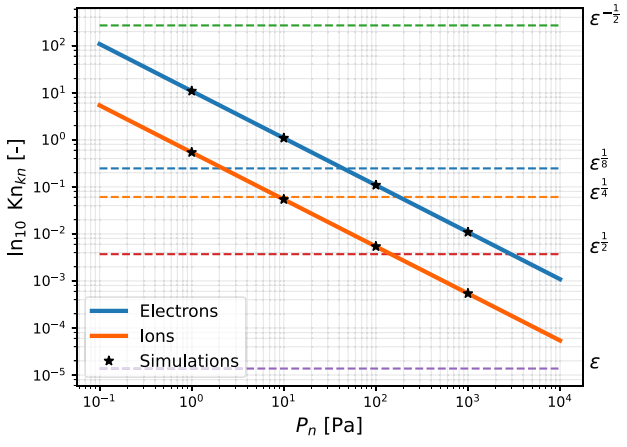

FIG. 5. Knudsen number for electrons (*blue*) and ions (*orange*) at different background gas pressures, with order of magnitudes highlighted in terms of powers of the mass ratio ε. The lengthscale $L_0 = L$ is the width of the domain, the characteristic length of the bulk. Simulation conditions are shown (*stars*).

In Fig. 7, we present the velocity profiles (u_k for **MF** and V_k for **DD**) throughout the domain and a view of the near wall region: the multifluid solution correctly captures the substantial absence of current in the quasineutral region for all pressure regimes, while the drift-diffusion model extends the acceleration region way beyond the theoretical sheath edge for low collisional plasmas. At a higher pressure, the **DD** model predicts the same flux of ions compared to the **MF** solution; the velocity of the electrons in the sheath presents a small discrepancy.

Figure 8 shows the profiles for the electric potential; similarly, the agreement of the two models increases with the neutral background pressure.

We can now use the information from the numerical simulations to obtain an estimation of the α parameter we introduced in Sec. III, propose a limit value of the Knudsen number that ensures equivalence of the two fluid models, and give a possible explanation for the discrepancies visible at a higher pressure.

B. Bridging multifluid and drift-diffusion

Figure 9 shows the velocity of the charges from the center of the domain until the wall, at different background pressures. We can see that the charge separation, at low pressures, happens when both velocities hit the collisionless Bohm speed $u_e = u_i = u_B$; as the Knudsen number decreases, the overall speed in the bulk diminishes. The velocity at the onset of the sheath is now better approximated by the

TABLE II. Knudsen number for electrons Kn$_{en}$ and ions Kn$_{in}$ and the ionization degree η at different background pressures. Characteristic lengthscale of the sheath is $L_0 = \lambda_D$, and bulk characteristic length is $L_0 = L$.

		Kn$_{en}$		Kn$_{in}$	
p_n	$\eta = \frac{n_{e0}}{n_n}$	Sheath	Bulk	Sheath	Bulk
1 Pa	$\sim 10^{-4}$	1143.47	11.43	56.82	0.568
10 Pa	$\sim 10^{-5}$	114.35	1.143	5.68	0.057
100 Pa	$\sim 10^{-6}$	11.43	0.114	0.568	5.68×10^{-3}
1000 Pa	$\sim 10^{-7}$	1.143	1.14×10^{-2}	5.68×10^{-2}	5.68×10^{-4}

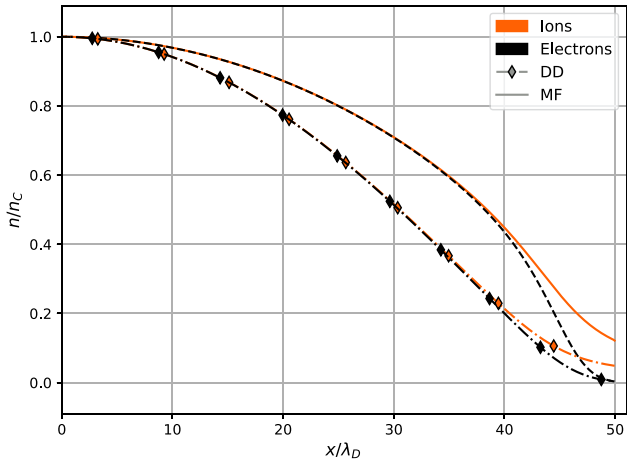

(a) 10 Pa

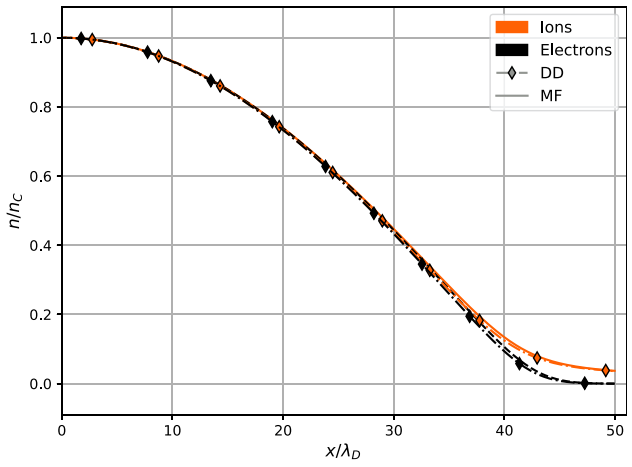

(b) 1000 Pa

FIG. 6. Number density of electrons and ions, scaled with the value at the center of the domain for different background pressures. Ions are in *orange* and electrons are in *black*. Multifluid solutions have no marker, and drift-diffusion ones are marked in *diamonds*. (a) 10 Pa and (b) 1000 Pa.

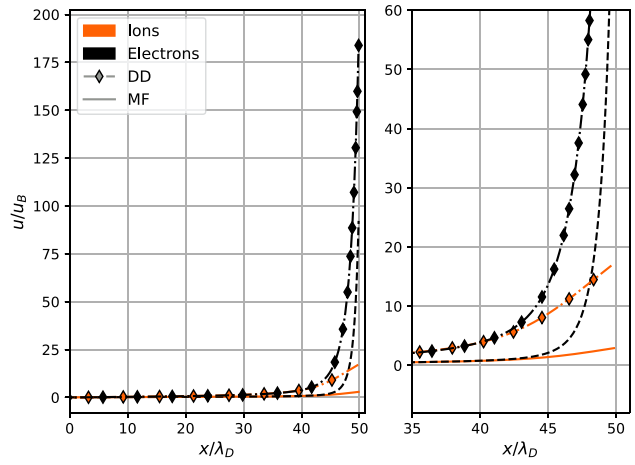

(a) 10 Pa

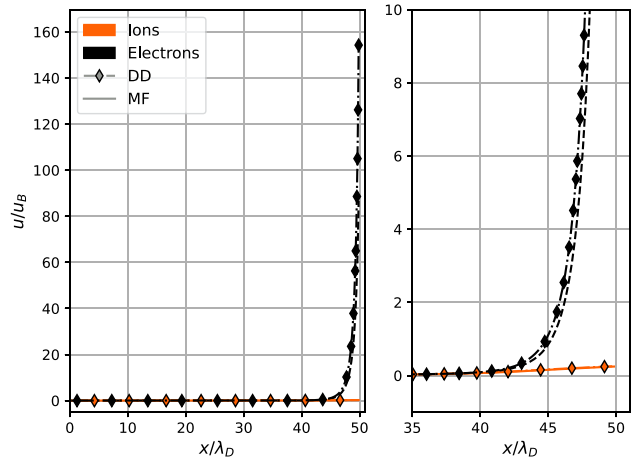

(b) 1000 Pa

FIG. 7. Charged species velocity for different background gas pressures, scaled with the Bohm velocity u_B. Each case comes with a close-up of the sheath region. Ions are in *orange* and electrons are in *black*. Multifluid solutions have no marker, and drift-diffusion ones are marked in *diamonds*. (a) 10 Pa and (b) 1000 Pa.

electrons Knudsen number Kn_{en}. We can propose a tentative definition of α that reflects this behavior,

$$\alpha = \min(\mathrm{Kn}_{en}, 1), \tag{28}$$

and obtain the final scaled version of Eqs. (9c) and (9d). Figure 10 shows the order of magnitude of the terms in those equations, for different values of a common Knudsen number $\mathrm{Kn} \sim \mathrm{Kn}_{en} \sim \mathrm{Kn}_{in}$. In the collisionless case, the term proportional to the collision frequency is null: the full electron momentum equation [Eq. (9c)] can be rearranged (remembering $\varepsilon \ll 1$), keeping the dominant pressure and electric field forcing terms, and integrated to obtain a relation for the electron number density,

$$n_e(\phi(x)) = n_C \exp[\phi(x)],$$

known as the Boltzmann relation for electrons.

When collisions are considered, we see that the corresponding term gains importance in both Eqs. (9c) and (9d). If we take a collisional "limit" $\mathrm{Kn} = \mathrm{Kn}_{en} = \mathrm{Kn}_{in} = \varepsilon^{1/2}$, we have

$$\partial_x\left[n_e\left(u_e^2 + \frac{1}{\varepsilon^2}\right)\right] = \frac{n_e}{\varepsilon^2}\partial_x\phi - \frac{16}{3\sqrt{2\pi}}\frac{n_e u_e}{\varepsilon^{3/2}}, \tag{29a}$$

$$\partial_x\left[n_i\left(u_i^2 + \frac{\kappa}{\varepsilon}\right)\right] = -\frac{n_i}{\varepsilon}\partial_x\phi - \frac{8}{3\sqrt{\pi}}\frac{n_i u_i\sqrt{\kappa}}{\varepsilon}. \tag{29b}$$

The value is chosen based on the results in Sec. VII A: for the argon plasma in object, $\varepsilon^{1/2} \sim 3.37 \times 10^{-3}$ approximates the Knudsen number of both species when the two models agree the most ($P_n = 1000$ Pa in Table II). If we rearrange Eq. (29), we obtain an expression for the two velocities,

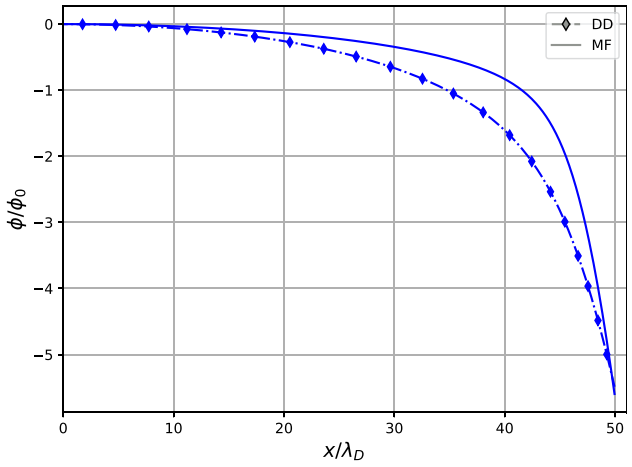

(a) 10 Pa

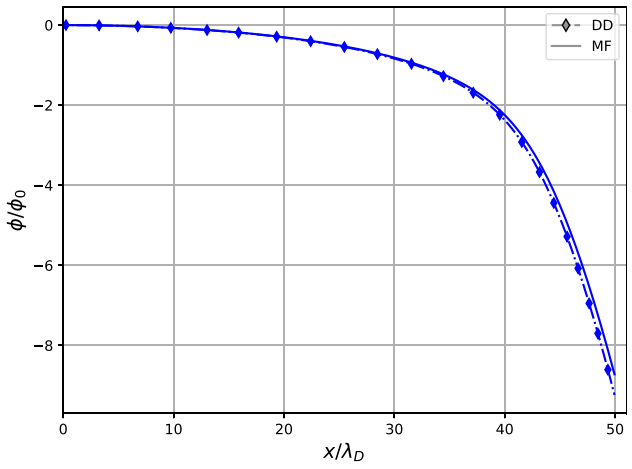

(b) 1000 Pa

FIG. 8. Electric potential profiles at different background gas pressures. Multifluid solutions have no marker, and drift-diffusion ones are marked in *diamonds*. (a) 10 Pa and (b) 1000 Pa.

$$u_e = \frac{3}{16}\left(\frac{2\pi}{\varepsilon}\right)^{1/2}\left(-\frac{\partial_x n_e}{n_e} + \partial_x\phi\right), \tag{30a}$$

$$u_i = \frac{3}{8}\left(\frac{\pi}{\kappa}\right)^{1/2}\left(-\kappa\frac{\partial_x n_i}{n_i} - \partial_x\phi\right). \tag{30b}$$

These expressions, coupled with Eqs. (9a), (9b), and (9e), give an equivalent set of equations to the drift-diffusion ones in the same limit. In fact, if we repeat the procedure starting from with Eq. (10), we obtain

$$V_e = \frac{3}{16}\left(\frac{2\pi}{\varepsilon}\right)^{1/2}\left(-\frac{\partial_x n_e}{n_e} + \partial_x\phi\right), \tag{31a}$$

$$V_i = \frac{3}{8}\left(\frac{\pi}{\kappa}\right)^{1/2}\left(-\kappa\frac{\partial_x n_i}{n_i} - \partial_x\phi\right), \tag{31b}$$

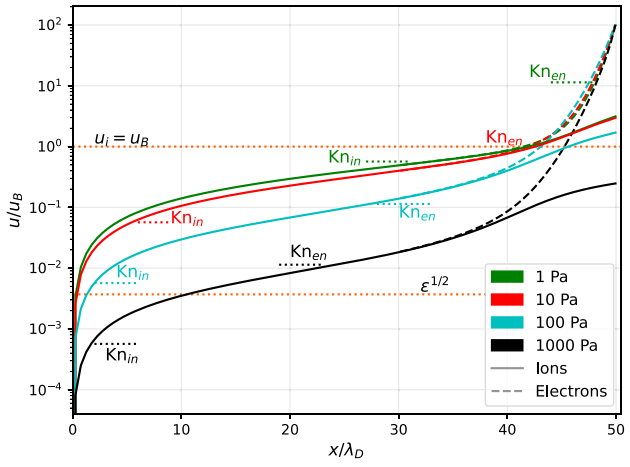

FIG. 9. Electrons (dashed) and ions (solid line) velocity obtained with multifluid simulations varying the background gas pressure (*green*: 1 Pa, *red*: 10 Pa, *cyan*: 100 Pa, and *black*: 1000 Pa). Orders of magnitude are highlighted with dotted lines compared to the mass ratio ε, the collisionless Bohm velocity u_B, and Knudsen numbers Kn_{en} and Kn_{in}.

the same expressions of Eq. (30). We proved that, provided that the elastic collisions with the background gas are frequent, the two models coincide. It is important to notice that the threshold value $\mathrm{Kn} = \varepsilon^{1/2}$ is uniquely defined by the choice of the species in the plasma; once the electron temperature T_e and the domain characteristic length are fixed, the simulation Knudsen number is set by the neutral background pressure through the neutral number density n_n appearing in Eq. (8). Additionally, we emphasize that $\mathrm{Kn} = \varepsilon^{1/2}$ corresponds to the continuum limit set by Graille *et al.*[19] to obtain fluid equations starting from the Boltzmann equation.

We can now explain also the small discrepancies at $P_n = 1000$ Pa: the assumption $\mathrm{Kn} < \varepsilon^{1/2}$ is valid only for the ions, while the electrons Knudsen number Kn_{en} remains slightly higher. It is likely that, by increasing the gas pressure, the dynamics of the electrons will become fully dominated by the elastic collisions and the distance of the models will reduce. A similar consideration can be done for the sheath, whose characteristic length is smaller ($L_0 = \lambda_D$) than the bulk one. From Table II, we see that the dynamics of the charged species in the sheath is collisionless, explaining the discrepancy between the two models in the region close to the walls.

The formulas derived in Sec. V to estimate the position of the sheath edge are tested in Sec. VII C.

C. Collisional sheath width

Figure 11 shows the prediction of the sheath width $w_s = |L/2 - x_s|$ in terms of the initial Debye length λ_D. The position of the sheath edge x_s is computed using Eqs. (17) and (19). We used here the value of the ionization frequency coming from the **DD** simulations. The reference ["density (reference)"] is taken as the point where the charge density in the numerical profile hits $n_e\bar{\rho}_C$, with $\bar{\rho}_C = 0.049$, i.e., the charge density at the position where $u_i = u_B$ in a collisionless **MF** simulation (in Beving *et al.*[32] it was set to $\bar{\rho}_C = 0.019$); the uncertainty of this value is related to the discretization of the sheath region and is below $0.1\lambda_D$. As expected, x^ρ can better approximate the creation of

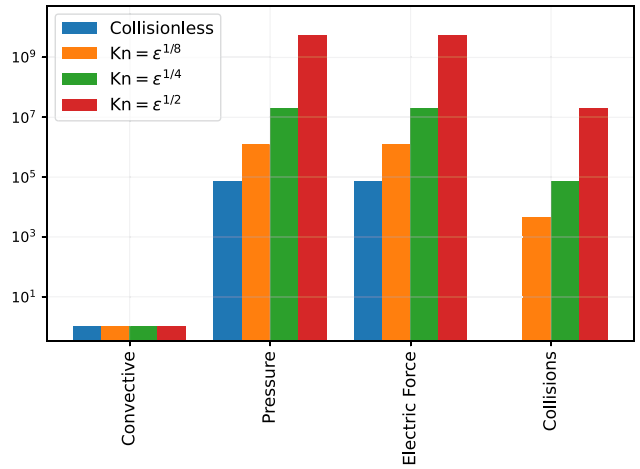

(a) Electrons.

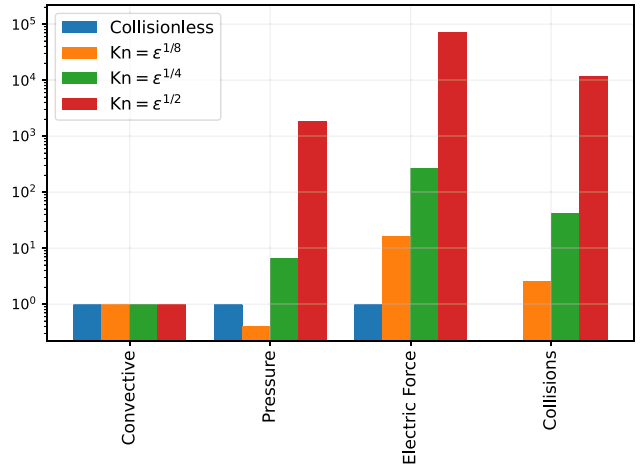

(b) Ions.

FIG. 10. Comparison of the order of magnitude of the different terms appearing in Eq. (9) (*top*: electrons and *bottom*: ions). The values are computed by varying the Knudsen number Kn, common to both charges. (a) Electrons and (b) ions.

the charge separation close to the wall than the value from the asymptotic procedure, with an error that gets smaller with the increase in the background pressure, approaching $\sim 1.5\lambda_D$. The prediction from Eq. (17) underestimates the width of the sheath, with an error that is constant around $7.5\lambda_D$; this result is a direct effect of the distance of the asymptote from the true point where the quasineutrality is broken. Figure 12 compares the prediction of Eq. (15) with the numerical results: one can see that the distance of the asymptote from the point the analytical profile departs the simulated profile is non-negligible.

The quality of the prediction of Eq. (19) and its sensitivity to the parameter $\bar{\rho}_C$ can be verified using analytical profiles for the sheath. Figure 13 shows the comparison of the numerical solution with the analytical profiles corresponding to the Mott–Gurney law,[9]

$$\phi(x) = -\sqrt{\frac{8 j_i \nu_{in}}{9\chi}} s^{3/2} \tag{32}$$

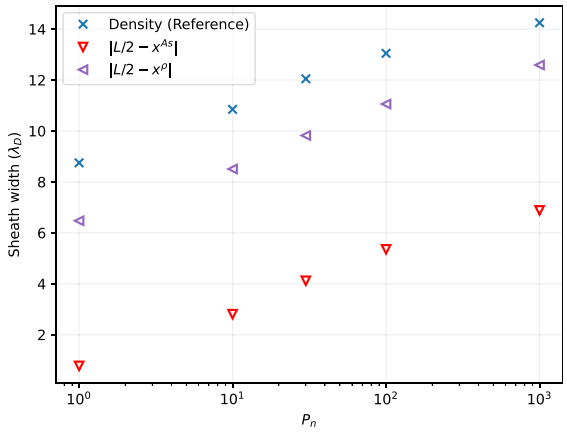

FIG. 11. Estimations of the sheath width for different background pressures width using three different approaches to obtain the sheath edge position: the position where the charge density for **DD** results equals $\bar{\rho}_C = 0.049$ ["density (reference)"], Eqs. (17) and (19) with $\bar{\rho}_C = 0.049$. x^{As} and x^{ρ} are computed using the ionization frequency from the drift-diffusion simulations.

with $j_i = n_i V_i$ the ion diffusion flux at the sheath edge and $s = [0, w_s]$ the adimensional sheath spatial coordinate. Two different threshold values have been used: Eq. (32) assumes zero electron population in the sheath; hence, it compares well when higher values of space charge $\bar{\rho}_C$ are considered.

At this point, one should test if the estimations obtained from the drift-diffusion governing laws can be transferred to the multifluid model. We use the formulas just derived using quantities from multifluid simulations (as the elastic collision frequencies are the same, this reduces to using the steady state value of the ionization frequency ν^{iz}). Figure 14 shows a comparison of x^{As} and x^{ρ} and three different references: (1) "Density (reference)," again the point where the charge density reaches the threshold value $\bar{\rho}_C$, (2) Beving *et al.*,[32] and (3) Baalrud *et al.*;[38] for (2) and (3), the sheath edge is taken as the position where

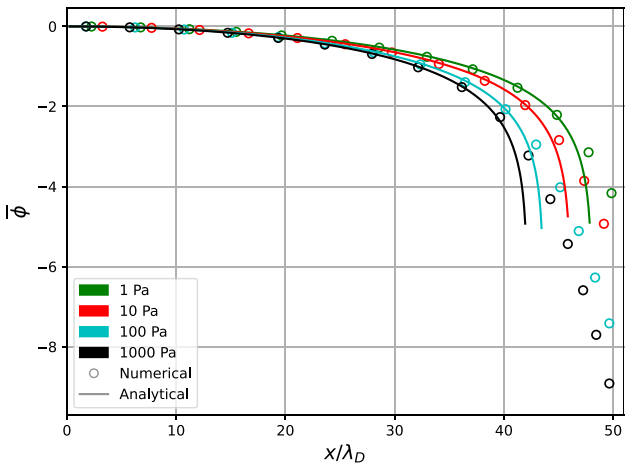

FIG. 12. Comparison of analytical profiles (*solid*) of the electric potential $\bar{\phi} = \phi/\phi_0$, obtained with Eq. (15) with numerical solutions (*circles*), at different background pressures.

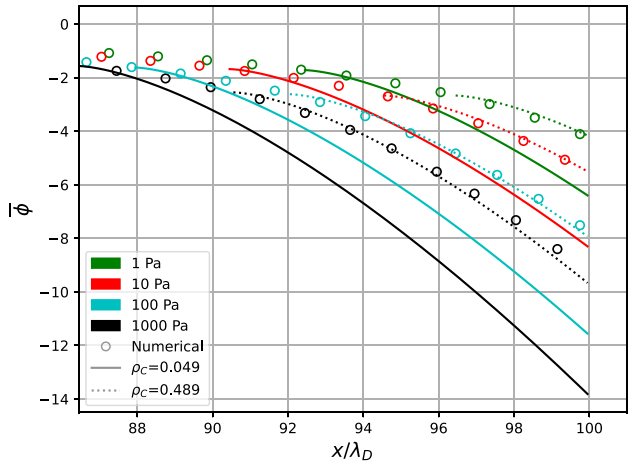

(a) Electric potential.

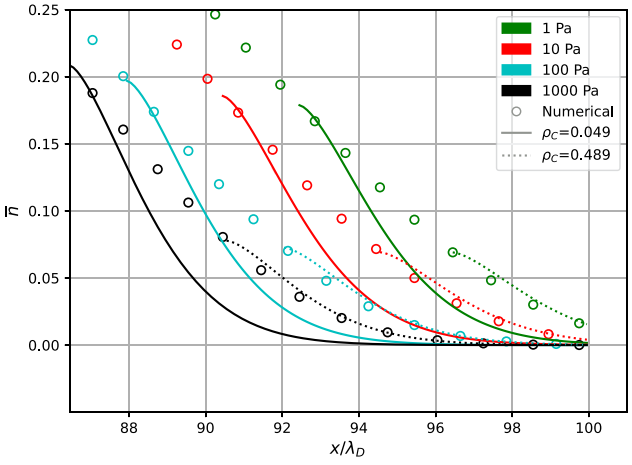

(b) Electron number density.

FIG. 13. Comparison of analytical profiles (*solid*) of the electric potential $\bar{\phi} = \phi/\phi_0$, obtained with Eq. (32), and electron number density $\bar{n} = n/n_0$ [obtained with Eqs. (16) and (32)] with numerical solutions (*circles*), at different background pressures. The sheath edge position, obtained with Eq. (19), is modified varying the imposed charge density $\bar{\rho}_C$. (a) Electric potential and (b) electron number density.

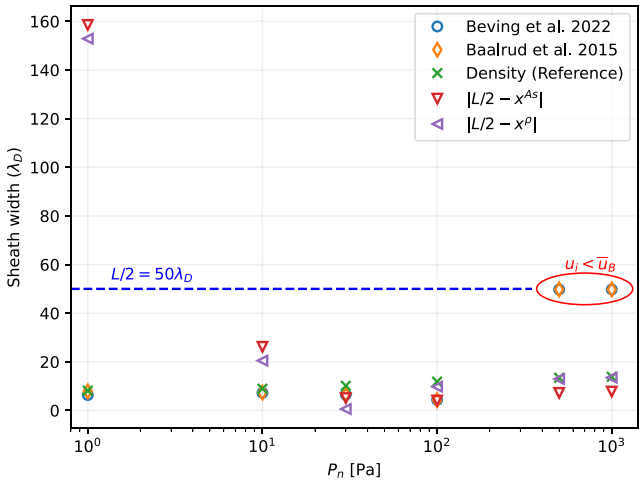

(a) Full.

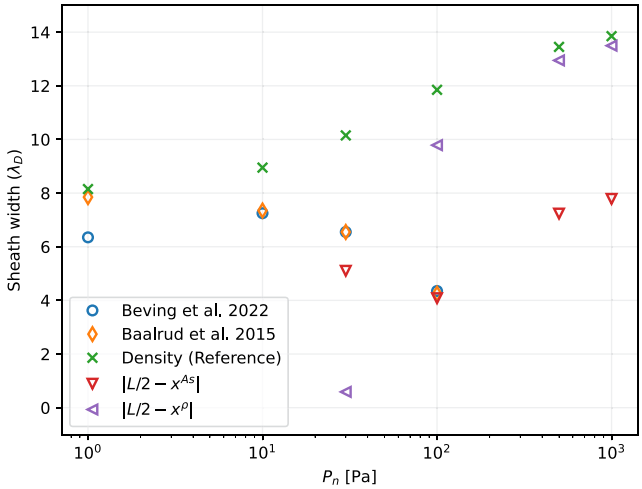

(b) Detail.

FIG. 14. Estimations of the sheath width for different background pressures width using five different approaches to obtain the sheath edge position: the position where the charge density for **MF** results equals $\bar{\rho}_C = 0.049$ ["density (reference)"], Baalrud *et al.*,[38] Beving *et al.*,[32] Eqs. (17) and (19) with $\bar{\rho}_C = 0.049$. x^{As} and x^{ρ} are computed using the ionization frequency from the multifluid simulations. (a) Full and (b) detail.

u_i equals a modified value of the Bohm speed u_B^{mod} that is obtained with, respectively,

$$u_B^{\text{mod}} = -10(\lambda_D/\lambda_{in}) + \sqrt{1 + 100(\lambda_D/\lambda_{in})^2} \tag{33}$$

and

$$u_B^{\text{mod}} = \sqrt{\frac{k_B(T_e + T_i) - m_e u_e^2}{m_i}} = \sqrt{(1+\kappa) - \varepsilon \bar{u}_e^2}\, u_B. \tag{34}$$

These three criteria have been chosen because they represent different approaches to the problem of finding a criterion for the sheath edge: one based on physical reasoning, one obtained from the Sagdeev potential,[39] and one that includes electron dynamics in the canonical Bohm criterion.

We can see that our proposed estimations improve when the Knudsen numbers of both species approach $\varepsilon^{1/2}$, with satisfying results for high background pressures ($P_n \sim 1000$ Pa). In the rarefied regime, the error is non-negligible, as expected. The two criteria taken from the literature have great accuracy at low pressures but fail to follow the behavior when this increases: Baalrud *et al.*[38] include in their modified Bohm criterion the electron dynamics but neglect the collisions; Beving *et al.*[32] included ion collisions effects but assumed cold ions[39] and constant ion mean free path while neglecting electron friction forces. In both these cases, $u_i < u_B^{\text{mod}}$ at a higher pressure, i.e., the modified Bohm speed that is proposed is never met by the ions; therefore, the last two values in Fig. 14 give a sheath with negligible width

($L/2 - w_s = L/2$). The results in Fig. 14 obtained with Eq. (33) differ from the one shown in Fig. 9 from the paper of Beving *et al.* This can be explained with the choice of units for the plot: in our work, the initial Debye length λ_D is the same for every background pressure, as both the initial electron temperature T_e and number density n_{e0} are fixed. In the reference work, the sheath width is shown in terms of Debye length at the center of the domain $\lambda_{D,c}$, a unit that is different for every collisional regime that they propose. Using data from Table II of the same reference, one can verify that $\lambda_{D,c}$ is almost one order of magnitude smaller at the highest background pressure condition than at the lowest one.

VIII. CONCLUSIONS

In this work, we proved, for the first time, the existence of a limit Knudsen number that results in the equivalence of the multifluid model and drift-diffusion approach, under the isothermal assumption. This value, which should be interpreted as an order of magnitude expressing a range of conditions rather than a strong upper limit, coincides with the square root of the electron-to-ion mass ratio, which is the Knudsen number for the continuum limit proposed by Graille *et al.*[19] in their kinetic derivation of multicomponent models for plasmas. We proved that, if a minimum collisionality is met, the multifluid equations naturally fall back to a multicomponent description of the plasma; in fact, the drift-diffusion equations in this work can be seen as a particular of the model in Graille *et al.*,[19] where only binary interactions are considered and with the movement of the particles described with respect to the laboratory reference frame (not moving).

The limit value was obtained by a non-dimensional analysis that included a novel scaling for the velocity of the charges in the bulk. Numerical simulation of an isothermal argon discharge showed great agreement for high background gas pressures ($P_n \gtrsim 1000$ Pa). After that, starting from the drift-diffusion equations, we obtain two formulas for *a priori* estimation of the sheath width: the first one is independent of any additional hypothesis, but it is less accurate; if we introduce an estimation of the charge separation,[32] we can improve the predicted value.

This work is open to further developments: higher pressure regimes should be investigated to confirm the intuitions coming from the high regime considered here; the isothermal condition should be lifted, introducing the effect of chemical reactions; more complex mixtures should be considered, moving to a full multicomponent-diffusion description. Finally, we considered for our simulations only the case of a sheath in front of a floating wall: other case should be considered, such as electron sheaths and double layers. In this latter case, for example, the characteristic length of the quasineutral region might be reduced, causing the Knudsen number to be larger, hence the equivalence to happen at higher background pressures.

ACKNOWLEDGMENTS

The first author is financed by the Fonds National de Recherche Scientifique (FNRS) through the FRIA grant. The support of CIEDS at Institut Polytechnique de Paris and Agence Innovation Défense in France (OPEN NUM DEF project, PI M. Massot) is gratefully acknowledged.

AUTHOR DECLARATIONS

Conflict of Interest

The authors have no conflicts to disclose.

Author Contributions

G. M. Gangemi: Conceptualization (equal); Data curation (lead); Formal analysis (lead); Investigation (lead); Methodology (equal); Visualization (lead); Writing – original draft (lead); Writing – review & editing (equal). **A. Alvarez Laguna:** Conceptualization (equal); Formal analysis (supporting); Methodology (equal); Writing – review & editing (equal). **M. Massot:** Conceptualization (equal); Formal analysis (supporting); Writing – review & editing (supporting). **K. Hillewaert:** Supervision (equal); Writing – review & editing (supporting). **T. Magin:** Conceptualization (equal); Formal analysis (supporting); Supervision (equal); Writing – review & editing (equal).

DATA AVAILABILITY

The data that support the findings of this study are available from the corresponding author upon reasonable request.

REFERENCES

[1]M. R. Carruth, Jr., J. A. Vaughn, R. T. Bechtel, and P. A. Gray, "Experimental studies on spacecraft arcing," J. Spacecr. Rockets **30**, 323–327 (1993).
[2]L. Uribarri and E. H. Allen, "Electron transpiration cooling for hot aerospace surfaces," in *20th AIAA International Space Planes and Hypersonic Systems and Technologies Conference, International Space Planes and Hypersonic Systems and Technologies Conferences* (American Institute of Aeronautics and Astronautics, 2015).
[3]E. Ahedo and F. I. Parra, "Partial trapping of secondary-electron emission in a Hall thruster plasma," Phys. Plasmas **12**, 073503 (2005).
[4]I. Hutchinson, *Principles of Plasma Diagnostics*, 2nd ed. (Cambridge University Press, 2002).
[5]S. Jubin, A. T. Powis, W. Villafana, D. Sydorenko, S. Rauf, A. V. Khrabrov, S. Sarwar, and I. D. Kaganovich, "Numerical thermalization in 2D PIC simulations: Practical estimates for low-temperature plasma simulations," Phys. Plasmas **31**, 023902 (2024).
[6]M. D. Acciarri, C. Moore, L. P. Beving, and S. D. Baalrud, "When should PIC simulations be applied to atmospheric pressure plasmas? Impact of correlation heating," Plasma Sources Sci. Technol. **33**, 035009 (2024).
[7]M. D. Acciarri, C. Moore, and S. D. Baalrud, "Artificial correlation heating in PIC simulations," Phys. Plasmas **31**, 093903 (2024).
[8]A. Alvarez Laguna, A. Lani, Y. Maneva, H. Deconinck, and S. Poedts, "Computational multi-fluid model for partially ionized and magnetized plasma," in *47th AIAA Plasmadynamics and Lasers Conference* (American Institute of Aeronautics and Astronautics, 2016).
[9]P. Chabert and N. Braithwaite, *Physics of Radio-Frequency Plasmas* (Cambridge University Press, 2011).
[10]A. Alvarez Laguna, T. Pichard, T. Magin, P. Chabert, A. Bourdon, and M. Massot, "An asymptotic preserving well-balanced scheme for the isothermal fluid equations in low-temperature plasmas at low-pressure," J. Comput. Phys. **419**, 109634 (2020).
[11]A. Alvarez Laguna, T. Magin, M. Massot, A. Bourdon, and P. Chabert, "Plasma-sheath transition in multi-fluid models with inertial terms under low pressure conditions: comparison with the classical and kinetic theory," Plasma Sources Sci. Technol. **29**, 025003 (2020).
[12]M. M. Becker and D. Loffhagen, "Enhanced reliability of drift-diffusion approximation for electrons in fluid models for nonthermal plasmas," AIP Adv. **3**, 012108 (2013).
[13]J. Teunissen, "Improvements for drift-diffusion plasma fluid models with explicit time integration," Plasma Sources Sci. Technol. **29**, 015010 (2020).
[14]H. Grad, "On the kinetic theory of rarefied gases," Commun. Pure Appl. Math. **2**, 331–407 (1949).
[15]V. Zhdanov, *Transport Processes in Multicomponent Plasma* (Taylor & Francis, 2002), Vol. 44.
[16]H. Struchtrup, *Macroscopic Transport Equations for Rarefied Gas Flows* (Springer, 2005).

[17]M. S. Benilov, "A kinetic derivation of multifluid equations for multispecies nonequilibrium mixtures of reacting gases," Phys. Plasmas **4**, 521–528 (1997).
[18]J. H. Ferziger and H. G. Kaper, *Mathematical Theory of Transport Processes in Gases* (American Elsevier Publishing Company, 1972).
[19]B. Graille, T. E. Magin, and M. Massot, "Kinetic theory of plasmas: Translational energy," Math. Models Methods Appl. Sci. **19**, 527–599 (2009).
[20]M. A. Lieberman and A. J. Lichtenberg, *Principles of Plasma Discharges and Materials Processing* (John Wiley & Sons, 2005).
[21]P. Chabert, "What is the size of a floating sheath?," Plasma Sources Sci. Technol. **23**, 065042 (2014).
[22]L. Tonks and I. Langmuir, "A general theory of the plasma of an arc," Phys. Rev. **34**, 876 (1929).
[23]D. Bohm, *The Characteristics of Electrical Discharges in Magnetic Fields* (McGraw-Hill, 1949).
[24]S. D. Baalrud, B. Scheiner, B. T. Yee, M. M. Hopkins, and E. Barnat, "Interaction of biased electrodes and plasmas: Sheaths, double layers, and fireballs," Plasma Sources Sci. Technol. **29**, 053001 (2020).
[25]M. Benilov, "The Child–Langmuir law and analytical theory of collisionless to collision-dominated sheaths," Plasma Sources Sci. Technol. **18**, 014005 (2009).
[26]T. E. Magin and G. Degrez, "Transport properties of partially ionized and unmagnetized plasmas," Phys. Rev. E **70**, 046412 (2004).
[27]J. B. Scoggins, V. Leroy, G. Bellas-Chatzigeorgis, B. Dias, and T. E. Magin, "Mutation++: MUlticomponent thermodynamic and transport properties for IONized gases in C++," SoftwareX **12**, 100575 (2020).
[28]J. P. Boeuf and L. C. Pitchford, "Two-dimensional model of a capacitively coupled rf discharge and comparisons with experiments in the Gaseous Electronics Conference reference reactor," Phys. Rev. E **51**, 1376–1390 (1995).
[29]V. V. Gorin, A. A. Kudryavtsev, J. Yao, C. Yuan, and Z. Zhou, "Boundary conditions for drift-diffusion equations in gas-discharge plasmas," Phys. Plasmas **27**, 013505 (2020).
[30]R. Sahu, A. R. Mansour, and K. Hara, "Full fluid moment model for low temperature magnetized plasmas," Phys. Plasmas **27**, 113505 (2020).
[31]K. U. Riemann, J. Seebacher, D. D. Tskhakaya, Sr., and S. Kuhn, "The plasma–sheath matching problem," Plasma Phys. Controlled Fusion **47**, 1949–1970 (2005).
[32]L. Beving, M. Hopkins, and S. Baalrud, "How sheath properties change with gas pressure: Modeling and simulation," Plasma Sources Sci. Technol. **31**, 084009 (2022).
[33]W. Schottky, "Diffusion theory of the positive column," Phys. Z. **25**, 635–640 (1924).
[34]K.-U. Riemann, "The influence of collisions on the plasma sheath transition," Phys. Plasmas **4**, 4158–4166 (1997).
[35]R. Leveque, *Numerical Methods for Conservation Laws* (Birkhäuser, 1992).
[36]M. Čada and M. Torrilhon, "Compact third-order limiter functions for finite volume methods," J. Comput. Phys. **228**, 4118–4145 (2009).
[37]G. Hagelaar, "Modelling methods for low-temperature plasmas," Technical Report (Université Paul Sabatier, 2008).
[38]S. D. Baalrud, B. Scheiner, B. Yee, M. Hopkins, and E. Barnat, "Extensions and applications of the Bohm criterion," Plasma Phys. Controlled Fusion **57**, 044003 (2015).
[39]J.-Y. Liu, Z.-X. Wang, and X. Wang, "Sheath criterion for a collisional sheath," Phys. Plasmas **10**, 3032–3034 (2003).